Method of random wave vectors in simulation of anisoplanatic effects.

V. V. Voitsekhovich [1], D. Kouznetsov [2], V. G. Orlov [1], and S. Cuevas [1]

[1] Instituto de Astronomia, UNAM. AP 70-264 Cd. Universitaria, 04510 Mexico D.F., Mexico.
[2] Centro de Instrumentos, UNAM. AP 70-186 Cd. Universitaria, 04510 Mexico D.F., Mexico.

Abstract

The feasibility of the method of random wave vectors (RWV) [1] for simulation of turbulence-induced anisoplanatic effects is discussed. The main advantage of RWV method over another approaches is that it allows to reproduce a very wide range of spacial frequencies in simulated processes overriding the restrictions imposed by the Nyquist limits. A simulation of the cross-correlated phase fluctuations produced by two initially plane waves propagating through the weak turbulence is considered. The variation of C_n^2 along a propagation path and an effect of finite outer scale of the turbulence are included in the simulation. The validity of the simulation is verified by comparison of theoretical and simulated results. The results obtained can be used in the problems related to adaptive optics, speckle inteferometry, guide stars and imaging through the turbulence.

1 Introduction

Anisoplanatic effects due to the atmospheric turbulence are of importance in many applications such as adaptive optics [2–5], guide stars [6–9], speckle interferometry [10–12], imaging through the turbulence [13–15], etc. The simulation of these effects is a powerful tool that can successively be used in the solution of both physical and technical problems related to the above areas.

The simulation of the effects of interest can be considered as a simulation of cross-correlated random processes with a given statistics. A suitable approach for such a simulation called the method of random wave vectors (RWV) has been suggested in [1] where it has been applied for the simulation of turbulence-induced amplitude and phase fluctuations. In this paper we use the RWV method for the simulation of cross-correlated phase fluctuations due to the propagation of two initially plane waves through the weak turbulence.

The plan of the paper is as follows. In Section 2, the theoretical spectra of phase fluctuations needed for simulation are derived. Section 3 describes the generalization of RWV method which allows to adjust it for the problem of interest. The validity of simulation is verified in Section 3 where the simulated results are compared to the theoretical ones. Section 4 is a summary of the results.

2 Theoretical correlations and cross-correlations.

In order to apply the RWV method for the simulation of anisoplanatic phenomena, one needs to know the spectra and the cross-spectrum of phase fluctuations at the observation plane. In the general case the spectra of interest follow from the solution of the so-called parabolic partial differential equation [16]. However in many cases of practical concern only the propagation through the weak turbulence is of interest when the approximated analytical Rytov solution of the parabolic equation is valid [16]. In this paper we restrict our attention to the simulation of correlated phase fluctuations due to the propagation of monohromatic light waves under the weak-turbulence conditions. So we derive below the necessary spectra in the Rytov approximation.

Let us consider two stars, say 1 and 2, separated by the angle γ. Assume that these stars produce two monohromatic, initially plane waves at the upper boundary of the atmosphere. Then, let us introduce the three-dimensional Cartesian coordinate system with the X and Y axes placed at the aperture plane. Without losing generality, we can assume that the first wave propagates along the Z-axis. In this case the fluctuations to be produced by the first star at the observation plane are expressed as [16]

$$\Psi_1(\mathbf{r}) = \chi_1(\mathbf{r}) + iS_1(\mathbf{r}) = ik\int_0^L \mathrm{d}z \int \mathrm{d}^2\kappa\; g_n(z,\boldsymbol{\kappa}) \exp\left(i\boldsymbol{\kappa}\cdot\mathbf{r} + \frac{\kappa^2 z}{2ik}\right), \tag{1}$$

where χ_1 and S_1 denote the log-amplitude and the phase fluctuations, respectively, $\mathbf{r}$ denotes the two-dimensional vector at the observation plane, k is the wavenumber, L is the propagation length, and g_n is the spectrum of fluctuations of the refractive-index random field.

Furthermore, let $\mathbf{n}$ be the unit propagation vector of the initially plane wave produced by the second star at the upper boundary of the atmosphere. The fluctuations to be produced by the second star at the observation plane are expressed as [17]

$$\Psi_2(\mathbf{r}) = \chi_2(\mathbf{r}) + iS_2(\mathbf{r}) = ik\int_0^L \mathrm{d}z \int \mathrm{d}^2\kappa g_n(z,\boldsymbol{\kappa}) \exp\left(i\boldsymbol{\kappa}\cdot\mathbf{r} + \frac{\kappa^2 z}{2ik} - i\boldsymbol{\kappa}\cdot\mathbf{n}_\perp z\right), \tag{2}$$

where $\mathbf{n}_\perp$ is the projection of the vector $\mathbf{n}$ on the observation plane.

Using Eqs.(1, 2), we can express the correlation functions $B_{S_1S_1}$, $B_{S_2S_2}$ and the cross-correlation function $B_{S_1S_2}$ of phase fluctuations as follows

$$B_{S_1S_1}(\rho) = B_{S_2S_2}(\rho) = 2\pi^2 k^2 \int_0^L \mathrm{d}z \int \mathrm{d}\kappa\kappa\Phi_n(z,\kappa)\, J_0(\kappa\rho)\left[\cos\left(\frac{\kappa^2 z}{k}\right) + 1\right] \tag{3}$$

$$B_{S_1S_2}(\boldsymbol{\rho}) = \langle S_1(\mathbf{r_1})\, S_2(\mathbf{r_2})\rangle = 2\pi^2 k^2 \int_0^L \mathrm{d}z \int \mathrm{d}\kappa\kappa\Phi_n(z,\kappa)\, J_0(\kappa\,|\boldsymbol{\rho} + \mathbf{n}_\perp z|)\left[\cos\left(\frac{\kappa^2 z}{k}\right) + 1\right] \tag{4}$$

where $\boldsymbol{\rho} = \mathbf{r_1} - \mathbf{r_2}$, $\langle\cdots\rangle$ denotes the statistical average, Φ_n is the isotropic spectrum of refractive-index fluctuations, ρ and κ denote the modules of the corresponding vectors, J_0 is the Bessel function, and $|\cdots|$ stands for the module of the vector $\boldsymbol{\rho} + \mathbf{n}_\perp z$.

The following equalities [16] have been used to get Eqs.(3, 4) from Eqs. (1, 2):

$$\begin{aligned}
\langle g_n(z_1,\boldsymbol{\kappa_1})\, g_n^*(z_2,\boldsymbol{\kappa_2})\rangle &= 2\pi\Phi_n(z_1,\boldsymbol{\kappa_1})\,\delta(z_1 - z_2)\,\delta(\boldsymbol{\kappa_1} - \boldsymbol{\kappa_2}),\\
\langle g_n(z_1,\boldsymbol{\kappa_1})\, g_n(z_2,\boldsymbol{\kappa_2})\rangle &= 2\pi\Phi_n(z_1,\boldsymbol{\kappa_1})\,\delta(z_1 - z_2)\,\delta(\boldsymbol{\kappa_1} + \boldsymbol{\kappa_2}),
\end{aligned}$$

where the sign $(*)$ stands for the complex conjugation, and δ is the Dirac delta-function.

Introducing the two-dimensional spectrum $W(\boldsymbol{\kappa})$ of the function $B(\boldsymbol{\rho})$ as:

$$W(\boldsymbol{\kappa}) = \frac{1}{2\pi} \int \mathrm{d}^2\rho \; B(\boldsymbol{\rho}) \exp(i\boldsymbol{\kappa} \cdot \boldsymbol{\rho}), \tag{5}$$

and applying the transformation (5) to Eqs. (3, 4), we get the following expressions for the spectra $W_{S_1S_1}$, $W_{S_2S_2}$ and for the cross-spectrum $W_{S_1S_2}$ of phase fluctuations

$$W_{S_1S_1}(\kappa) = W_{S_2S_2}(\kappa) = 2\pi^2 k^2 \int_0^L \mathrm{d}z \Phi_n(z,\kappa) \left[\cos\left(\frac{\kappa^2 z}{k}\right) + 1\right], \tag{6}$$

$$W_{S_1S_2}(\boldsymbol{\kappa}) = 2\pi^2 k^2 \int_0^L \mathrm{d}z \Phi_n(z,\kappa) \exp(-i\boldsymbol{\kappa} \cdot \mathbf{n}_\perp z) \left[\cos\left(\frac{\kappa^2 z}{k}\right) + 1\right]. \tag{7}$$

Eqs. (3, 4, 6, 7) present the general solution for arbitrary isotropic spectrum Φ_n of refractive-index fluctuations. This result is valid for the weak-turbulence conditions. In the following Sections we apply this general solution using the von Karmann refractive-index spectrum that gives us the possibility to include the outer-scale effects. In this case the spectrum Φ_n can be expressed as [18]:

$$\Phi_n(z,\kappa) = 0.033 C_n^2(z) \left(\kappa^2 + 1/L_0^2\right)^{-11/6}, \tag{8}$$

where $C_n^2(z)$ is the profile of the refractive-index structure characteristic, and L_0 denotes the outer scale of the turbulence.

Without loosing generality, we can rotate the coordinate system around Z-axis in such a way that $\mathbf{n}_\perp$ is expressed as:

$$\mathbf{n}_\perp = (\sin\gamma, 0), \tag{9}$$

where γ is the angular separation between two stars. From the physical point of view, this means that, in the rotated coordinates, the propagation vectors of both waves lie in XZ plane.

Substituting Eq. (8, 9) into Eqs. (3, 4, 6, 7), one can get the following final expressions.

The correlation and cross-correlation functions:

$$B_{S_1S_1}(\rho) = B_{S_2S_2}(\rho) = 0.132\pi^2 k^2 \int_0^L \mathrm{d}z C_n^2(z) \int_0^\infty \mathrm{d}\kappa\kappa \left(\kappa^2 + 1/L_0^2\right)^{-11/6} J_0(\kappa\rho), \tag{10}$$

$$\begin{aligned} &B_{S_1S_2}(\boldsymbol{\rho}) = 0.132\pi^2 k^2 \int_0^L \mathrm{d}z C_n^2(z) \int_0^\infty \mathrm{d}\kappa\kappa \left(\kappa^2 + 1/L_0^2\right)^{-11/6} J_0(\kappa r_+), \\ &r_+ = \sqrt{\rho^2 + z^2\sin^2\gamma + 2\rho z \sin\gamma\cos\varphi}, \end{aligned} \tag{11}$$

where φ denotes the polar angle of the vector $\boldsymbol{\rho}$.

The spectra and cross-spectrum:

$$W_{S_1S_1}(\kappa) = W_{S_2S_2}(\kappa) = 0.066\pi^2 k^2 \left(\kappa^2 + 1/L_0^2\right)^{-11/6} \int_0^L \mathrm{d}z C_n^2(z) \left[\cos\left(\frac{\kappa^2 z}{k}\right) + 1\right], \tag{12}$$

$$\begin{aligned} \mathrm{Re}\, W_{S_1S_2}(\boldsymbol{\kappa}) &= 0.066\pi^2 k^2 \left(\kappa^2 + 1/L_0^2\right)^{-11/6} \int_0^L \mathrm{d}z C_n^2(z) \cos(\kappa z \sin\gamma\cos\theta) \left[\cos\left(\tfrac{\kappa^2 z}{k}\right) + 1\right] \\ \mathrm{Im}\, W_{S_1S_2}(\boldsymbol{\kappa}) &= -0.066\pi^2 k^2 \left(\kappa^2 + 1/L_0^2\right)^{-11/6} \int_0^L \mathrm{d}z C_n^2(z) \sin(\kappa z \sin\gamma\cos\theta) \left[\cos\left(\tfrac{\kappa^2 z}{k}\right) + 1\right] \end{aligned} \tag{13}$$

where Re and Im denote the real and imaginary parts of complex quantity, and θ is the polar angle of the vector $\boldsymbol{\kappa}$.

In the derivation of Eqs. (10, 11) we have used the approximation $\cos\left(\frac{\kappa^2 z}{k}\right) \approx 1$ that holds with a good accuracy in problems related to the light propagation through the atmospheric turbulence [16]. However, for the sake of mathematical rigor and in order to be able to check this approximation by the simulation, we keep this term unchanged in expressions (12, 13) for the spectra and cross-spectrum which will be used in the simulation.

As one can see from (11, 13), despite of the isotropy of refractive-index spectrum (9), the corresponding cross-correlation function (11) is anisotropic although still homogeneous. As a consequence of this anisotropy, the cross-spectrum (13) is the complex-valued function. We describe in the following Sections the generalization of RWV method that allows to simulate such processes.

3 Simulation method: theoretical derivations

In Ref. 1 the RWV method has been applied for the relative simple case when the cross-spectrum of the simulated processes is a real-valued non-negative function. We present below such a generalization of RWV method which allows to simulate the random processes with a more complicate cross-spectrum.

As it has been shown in Section 2, the processes to be simulated have the following salient features.

1. Both processes are isotropic.
2. The spectra of both processes are equal, real-valued functions.
3. The cross-spectrum is the complex-valued function.

To take into account the properties above, the phase fluctuations S_1 and S_2 at the observation plane are simulated as follows

$$\begin{aligned} S_1(\mathbf{r}) &= \sum_{m=1}^{M} F(p_m) \cos(\mathbf{p}_m \cdot \mathbf{r} + \varphi_m), \\ S_2(\mathbf{r}) &= \sum_{m=1}^{M} F(p_m) \cos[\mathbf{p}_m \cdot \mathbf{r} + \varphi_m + a(\mathbf{p}_m)\psi_m + b(\mathbf{p}_m)]. \end{aligned} \tag{14}$$

In what follows the modules p_m and the orientations θ_m of the vectors $\mathbf{p}_m$, and the phases φ_m and ψ_m are considered as statistically independent quantities. By definition, θ_m and φ_m are assumed to be distributed uniformly inside the range $[-\pi, \pi]$, while ψ_m are distributed uniformly inside the range $[-1, 1]$.

We choose the functions $F(p_m)$, $a(\mathbf{p}_m)$, and $b(\mathbf{p}_m)$ in such a way that the theoretical correlation and cross-correlation functions (10, 11) coincide with the corresponding functions following from (14). Using the same development as in Ref. 1, one can write a condition of coincidence as

$$B_{S_1 S_1}(\rho) = B_{S_2 S_2}(\rho) = \frac{1}{2} \sum_{m=1}^{M} \left\langle F^2(p_m) \cos(\mathbf{p}_m \cdot \boldsymbol{\rho}) \right\rangle, \tag{15}$$

$$B_{S_1 S_2}(\boldsymbol{\rho}) = \frac{1}{2} \sum_{m=1}^{M} \left\langle F^2(p_m) \cos[\mathbf{p}_m \cdot \boldsymbol{\rho} - a(\mathbf{p}_m)\psi_m - b(\mathbf{p}_m)] \right\rangle. \tag{16}$$

Applying the transformation (5) to Eqs. (15, 16), we get

$$
\begin{aligned}
&W_{S_1S_1}(\kappa) = \frac{\pi}{2}\sum_{m=1}^{M}\int \mathrm{d}^2 p_m\ F^2(p_m)\,\Omega(\mathbf{p}_m)\left[\delta(\mathbf{p}_m+\boldsymbol{\kappa})+\delta(\mathbf{p}_m-\boldsymbol{\kappa})\right],\\
&W_{S_1S_2}(\boldsymbol{\kappa}) = \frac{\pi}{2}\sum_{m=1}^{M}\int \mathrm{d}\psi_m\ \eta(\psi_m)\int \mathrm{d}^2 p_m F^2(p_m)\,\Omega(\mathbf{p}_m)\times\\
&\left\{\exp\left\{-i\left[a(\mathbf{p}_m)\,\psi_m+b(\mathbf{p}_m)\right]\right\}\delta(\mathbf{p}_m+\boldsymbol{\kappa})+\exp\left\{i\left[a(\mathbf{p}_m)\,\psi_m+b(\mathbf{p}_m)\right]\right\}\delta(\mathbf{p}_m-\boldsymbol{\kappa})\right\},
\end{aligned}
\tag{17}
$$

where Ω and η are the probability density functions (PDF) of the vector $\mathbf{p}_m$ and ψ_m, respectively. Note that there is a misprint in Ref. 1: the coefficient π in Eqs. (6, 9,10, 11) has to be replaced by $\pi/2$.

Since the processes under simulation are isotropic, the PDF Ω can also be chosen as an isotropic function, i.e. $\Omega(\boldsymbol{\kappa}) = \Omega(\kappa)$. Performing the integration over p_m and the summation over m, we get

$$
F(\kappa) = \sqrt{\frac{W_{S_1S_1}(\kappa)}{\pi M\Omega(\kappa)}},
\tag{18}
$$

$$
\tfrac{1}{2}\int \mathrm{d}\psi\eta(\psi)\left\{\exp\left\{-i\left[a(-\boldsymbol{\kappa})\,\psi+b(-\boldsymbol{\kappa})\right]\right\}+\exp\left\{i\left[a(\boldsymbol{\kappa})\,\psi+b(\boldsymbol{\kappa})\right]\right\}\right\} = \frac{W_{S_1S_2}(\boldsymbol{\kappa})}{W_{S_1S_1}(\kappa)},
\tag{19}
$$

In what follows we seek the functions $a(\boldsymbol{\kappa})$ and $b(\boldsymbol{\kappa})$ as odd functions of the vector $\boldsymbol{\kappa}$, i.e.

$$
a(-\boldsymbol{\kappa}) = -a(\boldsymbol{\kappa}),\ \ b(-\boldsymbol{\kappa}) = -b(\boldsymbol{\kappa}).
\tag{20}
$$

Substituting Eq. (20) into Eq. (19), and recalling that ψ is distributed uniformly inside the range $[-1,1]$ by definition, we have the following equations for the functions a and b

$$
\begin{aligned}
&\tfrac{1}{2}\int_{-1}^{1}\mathrm{d}\psi\cos\left[a(\boldsymbol{\kappa})\,\psi+b(\boldsymbol{\kappa})\right] = \frac{\sin\left[a(\boldsymbol{\kappa})\right]\cos\left[b(\boldsymbol{\kappa})\right]}{a(\boldsymbol{\kappa})} = w_r(\boldsymbol{\kappa}),\\
&\tfrac{1}{2}\int_{-1}^{1}\mathrm{d}\psi\sin\left[a(\boldsymbol{\kappa})\,\psi+b(\boldsymbol{\kappa})\right] = \frac{\sin\left[a(\boldsymbol{\kappa})\right]\sin\left[b(\boldsymbol{\kappa})\right]}{a(\boldsymbol{\kappa})} = w_i(\boldsymbol{\kappa}),\\
&w_r(\boldsymbol{\kappa}) = \frac{\mathrm{Re}\,W_{S_1S_2}(\boldsymbol{\kappa})}{W_{S_1S_1}(\kappa)},\ \ w_i(\boldsymbol{\kappa}) = \frac{\mathrm{Im}\,W_{S_1S_2}(\boldsymbol{\kappa})}{W_{S_1S_1}(\kappa)}.
\end{aligned}
\tag{21}
$$

The solution of (21) satisfying the conditions (20) is given by

$$
\begin{aligned}
&b(\boldsymbol{\kappa}) = \mathrm{atan2}\left[w_i(\boldsymbol{\kappa}), w_r(\boldsymbol{\kappa})\right],\\
&a(\boldsymbol{\kappa}) = \mathrm{asinc}\left(w_r(\boldsymbol{\kappa})/\cos(b(\boldsymbol{\kappa}))\right)\mathrm{sign}\left(\sin\theta\right),
\end{aligned}
\tag{22}
$$

where the function atan2(y,x) returns the arc tangent of y/x in the range -π to π, asinc(y) is the solution of the equation $\sin(x)/x = y$ in the range $[0,\pi]$, the function sign(x) returns the sign of x, and θ is the angle of the vector $\boldsymbol{\kappa}$.

The use of the function atan2 in Eq. (22) instead of the conventional arc tangent allows to get a solution for $b(\boldsymbol{\kappa})$ to be valid for both positive and negative w_r and w_i. The function $b(\boldsymbol{\kappa})$ given by (22) is always the odd function of $\boldsymbol{\kappa}$ because, as it follows from Eqs. (12, 13), the real and the imaginary parts of the cross-spectrum $W_{S_1S_2}(\boldsymbol{\kappa})$ are the even and the odd functions of the vector $\boldsymbol{\kappa}$, respectively. The function sign$(\sin\theta)$ in Eq. (22) gives the solution for the function $a(\boldsymbol{\kappa})$ satisfying

the condition (20). From the computational point of view, it is sufficient to find $z(\boldsymbol{\kappa})$ as a solution of Eq. (22a) inside the range $[0, \pi]$.

Let us choose now the PDF $\Omega(\kappa)$. Since both processes have the same spectra, we can choose the PDF $\Omega_\kappa(\kappa)$ of the module of vector $\boldsymbol{\kappa}$ matching to the spectrum (12). From the viewpoint of simulation accuracy, the best choice is to take Ω_κ proportional to the square root of $W_{S_1S_1}(\kappa)$ given by Eq. 12. Such a distribution can be generated making use of, for example, the rejection method [19]. However it is not very convenient from the computational point of view because it will make the simulation slower. So, it is preferable to choose a PDF that, on the one hand, would give a suitable approximation for the square root of (12) and, on the other hand, that the indefinite integral of this function would be known analytically and would be analytically invertible. Taking into account the above consideration, we choose the Lorentzian PDF [19] as follows:

$$\Omega_\kappa(\kappa) = \frac{1}{\Omega_0(\kappa^2 + 1/L_0^2)}, \quad \Omega_0 = L_0\left[\arctan(K_2 L_0) - \arctan(K_1 L_0)\right], \tag{23}$$

where K_1 and K_2 are the lower and the upper boundaries of the region of spacial frequencies inside which the phase fluctuations are simulated. By definition, the PDF $\Omega_\kappa(\kappa)$ is considered to be equal to zero outside the above region.

The corresponding PDF $\Omega(\kappa)$ of the vector $\boldsymbol{\kappa}$ is given by

$$\Omega(\kappa) = \frac{1}{2\pi\Omega_0\kappa(\kappa^2 + 1/L_0^2)}. \tag{24}$$

Making use of the considerations above, the samples S_1 and S_2 are simulated as follows.

1. The set $\{s_m\}$ of M random numbers s_m distributed uniformly inside the range $[0, 1]$ is generated. Then, in order to get the set of $\{p_m\}$ distributed with the PDF (23), the following transformation is applied:

$$p_m = \frac{1}{L_0}\tan\left\{s_m L_0\left[\arctan(K_2 L_0) - \arctan(K_1 L_0)\right]\right\}. \tag{25}$$

Generating M random, uniformly distributed inside the range $[-\pi, \pi]$ angles θ_m of p_m, we obtain M random vectors $\mathbf{p}_m$ with PDF given by Eq. (24).

2. Making use of the sets $\{p_m\}$ and $\{\theta_m\}$ simulated at the step 1, we calculate the magnitudes of $W_{S_1S_1}(p_m)$, $W_{S_1S_2}(\mathbf{p}_m)$, and $\Omega(p_m)$. Substituting $W_{S_1S_1}(p_m)$ and $\Omega(p_m)$ into Eq. (18), we get the amplitudes $F(p_m)$.

3. The magnitudes of functions $a(\mathbf{p}_m)$ and $b(\mathbf{p}_m)$ are calculated from Eq. (22) using the magnitudes $W_{S_1S_1}(p_m)$ and $W_{S_1S_2}(\mathbf{p}_m)$ obtained at the step 2.

4. M random, uniformly distributed inside the range $[-\pi, \pi]$ magnitudes of φ_m are generated.

5. M random, uniformly distributed inside the range $[-1, 1]$ magnitudes of ψ_m are generated.

6. Substituting the sets of $\{F(p_m)\}$, $\{\mathbf{p}_m\}$, $\{a(\mathbf{p}_m)\}$, $\{b(\mathbf{p}_m)\}$, $\{\varphi_m\}$, and $\{\psi_m\}$ into Eq. (14), the samples $S_1(\mathbf{r})$ and $S_2(\mathbf{r})$ can be calculated at any chosen grid of coordinates $\mathbf{r}$.

The simulation can be accelerated if $M/2$ vectors $\mathbf{p}_m$ $(m = 1, .., M/2)$ are simulated, while the remaining $M/2$ vectors $\mathbf{p}_m$ $(m = M/2, .., M)$ are taken as $\mathbf{p}_{m+M/2} = -\mathbf{p}_m$ $(m = 1, .., M/2)$. In this case we need to calculate $a(\mathbf{p}_m)$ and $b(\mathbf{p}_m)$ only $M/2$ times and then to change their signs to get $a(-\mathbf{p}_m)$ and $b(-\mathbf{p}_m)$. Note that in this approach M random φ_m and ψ_m have to be simulated.

4 Comparison of simulated and theoretical results

In order to demonstrate the efficiency of the above method, we compare in this Section the theoretical and simulated statistical characteristics of phase fluctuations. In this paper we use the Hufnagel C_n^2 profile [20] for calculation of the theoretical expressions (10-13):

$$C_n^2(z) = C_0\, r_0^{-5/3} k^{-2} \left[\left(\frac{z}{z_0} \right)^{10} \exp\left\{ -\frac{z}{z_1} \right\} + \exp\left\{ -\frac{z}{z_2} \right\} \right], \tag{26}$$

where r_0 is the Fried parameter, $C_0 = 1.027 \times 10^{-3}$ m^{-1} , $z_0 = 4.632 \times 10^3$ m , $z_1 = 10^3$ m , $z_2 = 1.5 \times$

In Eq. (26), the altitude z and the Fried parameter r_0 are given in meters, the wavenumber k is given in inverse meters, and the units of C_n^2 are meters to the power $-2/3$.

Although the results of this Section are based on the calculations with the von Karmann refractive-index spectrum and the Hufnagel C_n^2 profile, any another spectrum or profile, either theoretical or experimental, can easily be used in the simulation.

The simulated statistical characteristics are compared to the theoretical ones in Figs. 1-3. The simulation parameters which are common for all the graphs are the following: the number of harmonics $N = 100$, the frequency limits: $K_1 = 0$, $K_2 = 10^4$ 1/m , the number of samples used for averaging is equal to 5000. The rest of parameters are indicated in the figures.

Figs. 1-2 compare the theoretical cross-structure functions $D_{S_1S_2}$ to the simulated ones. As it has been shown in Section 2, the function $D_{S_1S_2}$ is anisotropic but still homogeneous, i.e.

$$D_{S_1S_2}(\mathbf{r_1}, \mathbf{r_2}) = \left\langle [S_1(\mathbf{r_1}) - S_2(\mathbf{r_2})]^2 \right\rangle = D_{S_1S_2}(\mathbf{r_1} - \mathbf{r_2}) = D_{S_1S_2}(\rho, \varphi),$$

where $\rho = |\mathbf{r_1} - \mathbf{r_2}|$, and φ is the polar angle of the vector $\mathbf{r_1} - \mathbf{r_2}$.

So, the cross-structure function $D_{S_1S_2}$ can be considered as a function of two arguments: the separation ρ between the two observation points and the angle φ. Fig. 1 plots this function for different star separations γ for fixed $\varphi = 0$, while Fig. 3 shows how the simulation handles the anisotropy in the cross-structure function (the dependance on the angle φ). One can see a good agreement between the theoretical and simulated results which takes place even for big separations between the observation points.

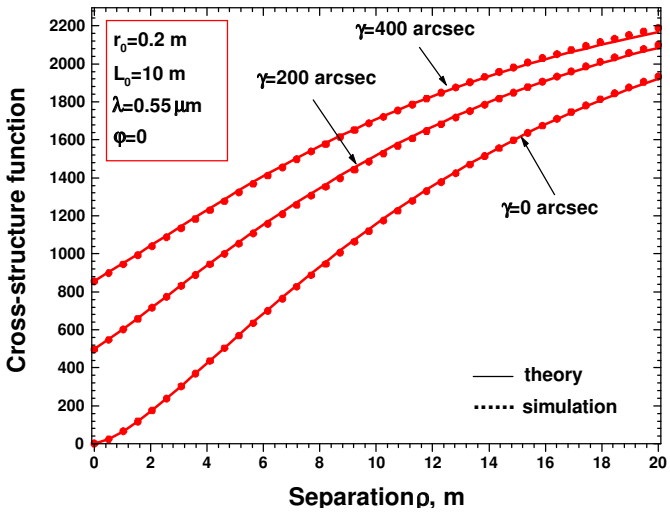

Fig.1. Theoretical and simulated cross-structure functions.

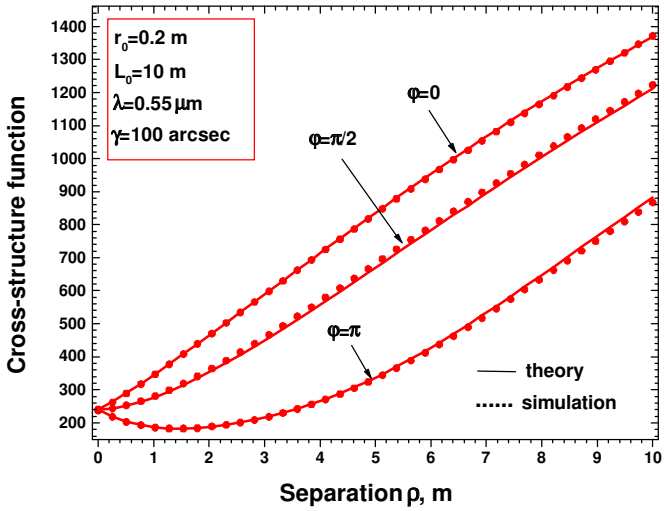

Fig.2. Anisotropy in cross-structure functions.

In some applications the residual structure function

$$D_{S_R}(\mathbf{r_1}, \mathbf{r_2}) = \left\langle [S_R(\mathbf{r_1}) - S_R(\mathbf{r_2})]^2 \right\rangle, \; S_R(\mathbf{r}) = S_1(\mathbf{r}) - S_2(\mathbf{r})$$

is of interest. Fig. 3 illustrates how this function is reproduced in the simulation.

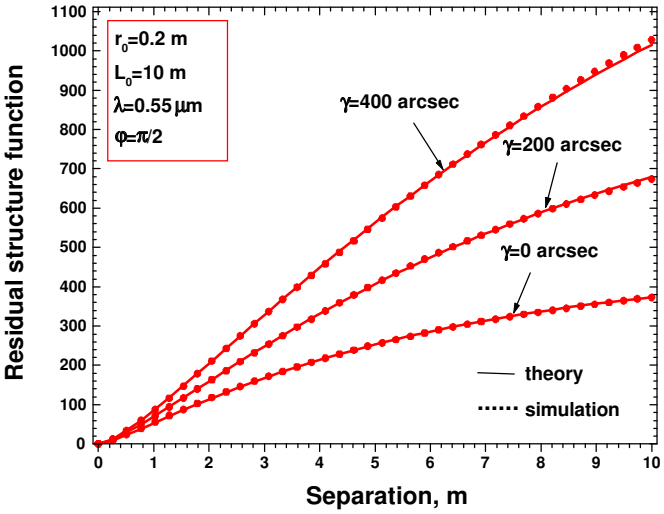

Fig. 3. Theoretical and simulated residual structure functions.

The results of this Section show that the simulation reproduces with a good accuracy the theoretical cross-structure functions. It means from the physical viewpoint that simulated samples have the desired second-order statistics.

In some applications (for example, in speckle interferometry) the simulation of the total wave field rather than the simulation of phase fluctuations is of interest. Since under the weak-turbulence conditions the effects of amplitude fluctuations are practically negligible [10], the samples of wave field $U(\mathbf{r})$ can be calculated through the samples of phase fluctuations S_1 and S_2 as follows

$$U(\mathbf{r}) = A_1 \exp[iS_1(\mathbf{r})] + A_2 \exp[iS_2(\mathbf{r}) + i\kappa \mathbf{r} \cdot \mathbf{n}_\perp],$$

where A_1 and A_2 are the amplitudes of two waves, and $\mathbf{n}_\perp$ is given by Eq. (9).

5 Summary

The application of RWV method for the simulation of anisoplanatic effects has been suggested. The general theoretical expression needed for such type of simulation have been derived. The efficiency of the method has been illustrated by the comparison of the theoretical and simulated results. Although a particular refractive-index spectrum and C_n^2 profile have been used in the present simulation, any another models, both theoretical and experimental as well, can easily be applied using the general expressions (6, 7).

The simulation results have shown a good coincidence of theoretical and simulated cross-structure functions for both small and big separations between the observation points. It means that the RWV method allows one to reproduce a very wide range of spatial frequencies in simulated processes using a relatively small number of harmonics (we recall that only 100 harmonics have been used in the present simulation). This noticeable property of RWV method is easily explicable if one compares it to the conventional approaches. Similar to the conventional methods, the RWV method suggests to construct the simulated process through its expansion in the domain of spatial frequencies (in other words, as a linear combination of frequency harmonics). However, in other methods the frequency limits within which the simulation can be performed, the discrete frequency grid, and a number of harmonics as well are always uniquely determined by the spatial grid. In other words, the wider is a desired frequency range, the greater number of harmonics has to be used in simulation. Contrary to this, the RWV method uses more flexible approach, and the main difference is in the choice of discrete frequencies. These frequencies (called as random wave vectors) are not related to the spatial grid. Instead they are generated randomly with a distribution matching to the spectrum of simulated process. The limits within which random wave vectors are generated can be chosen arbitrary. In result, the processes with very wide spectra can be simulated using a relatively small number of harmonics.

6 Acknowledgments

This work was supported by Consejo Nacional de Ciencia y Tecnologia (Mexico) project 1020P-E9507 and by Sistema Nacional de Investigadores (Mexico).

References

[1] D. Kouznetsov, V. V. Voitsekhovich, and R. Ortega-Martinez, "Simulation of turbulence-induced phase and log-amplitude distortions," Appl. Opt. **36**, 464-469 (1997).

[2] J .H. Shapiro, "Propagation-medium limitations on phase-compensated atmospheric imaging", J. Opt. Soc. Am., **66**, 460-469 (1976).

[3] D. L. Fried, "Anisoplanatism in adaptive optics", J. Opt. Soc. Am. **72**, 52-61 (1982).

[4] M. C. Roggermann, B. M. Welsh, D. Montera, and T. A. Rhoadarmer, "Method for simulating atmospheric turbulence phase effects for multiple time slices and anisoplanatic conditions," Appl. Opt. **34**, 4037-4051 (1995).

[5] M. C. Roggermann, B. M. Welsh, and R. Q. Fugate, "Improving the resolution of ground-based telescopes," Rew. Mod. Phys., **69**, 437-505 (1997).

[6] R. Foy, and A. Laberye, "Feasibility of adaptive telescope with laser probe," Astron. Astrophys., **152**, L29-L31 (1985).

[7] M. Tallon, and R Foy, "Adaptive telescope with laser probe: isoplanatism and cone effect," Astron. Astrophys., **235**, 549-557 (1990).

[8] B. M. Welsh, and C. S. Gardner, "Effects of turbulence-induced anisoplanatism on the imaging performance of adaptive-astronomical telescopes using laser guide stars," J. Opt. Soc. Am. A, **8**, 69-80 (1991).

[9] D. L. Fried, "Focus anisoplanatism in the limit of infinitely many artificial-guide-star reference spots," J. Opt. Soc. Am. A, **12**, 939-949 (1995).

[10] F. Roddier, "The effects of atmospheric turbulence in optical astronomy," In. *Progress in Optics,* v. **19**, 281-376 (1981).

[11] J .C. Dainty, "The transfer function, signal-to-noise ratio, and limiting magnitude in stellar speckle interferometry," Mon. Not. R. Astron. Soc. **169**, 631-641 (1974).

[12] F. Roddier, J. M. Gilli, and J. Vernin, "On the isoplanatic patch size in stellar speckle interferometry," J. Opt. (Paris) **13**, 63-70 (1982).

[13] M .C. Roggermann, E. L. Caudill, D. W. Tylper, M. J. Fox, M. A. Von Bokern, and L. C. Matson, "Compensated speckle imaging: theory and experimental results," Appl. Opt. **33**, 3099-3110 (1994).

[14] J. C. Ricklin, M. A. Vorontsov, G. W. Carhart, D. Gose, and W. B. Miller, "Turbulent phase screen for study of imaging system performance," J. Mod. Opt. **42**, 13-17 (1995).

[15] M. A. Vorontsov, G. W. Carhart, D. V. Pruidze, J. C. Ricklin, and D. G. Voelz, "Image quality criteria for an adaptive imaging system based on statistical analysis of the speckle field," J. Opt. Soc. Am. A, **13**, 1456-1466 (1996).

[16] V. I. Tatarski, *The Effects of the Turbulent Atmosphere on Wave Propagation* (National Science Foundation Report TT-68-50464, 1968).

[17] E. A. Vitrichenko , V. V. Voitsekhovich, M. I. Mishchenko , "Effect of atmospheric turbulence on the size of the field of view of adaptive systems," USSR Academy of Sciences: Atmospheric and Oceanic Physics, **20**, 870-872 (1984).

[18] G. W. Reinhardt, and S .A. Collins, "Outer scale effects in turbulence-degraded light-beam spectra," J. Opt. Soc. Am. **62,** 1526-1528 (1972).

[19] W. H. Press, B. P. Flannery, S. A. Teukolsky, and W. T. Vetterling, *Numerical Recipes in C,* Second Edition, Ch. 7 (Cambridge University Press, Cambridge, 1995).

[20] R. E. Hufnagel, "Variation of atmospheric turbulence," in *Optical Propagation through Turbulence*, OSA Technical Digest Series (OSA, Washington, D.C., 1974), p.WA1-1 – WA1-4.